Ambient-temperature liquid jet targets for high-repetition-rate HED discovery science

F. Treffert,[1,2,a)] G. D. Glenn,[1,3,a)] H.-G. J. Chou,[1,4] C. Crissman,[1,5] C. B. Curry,[1,6] D. P. DePonte,[1] F. Fiuza,[1] N. J. Hartley,[1] B. Ofori-Okai,[1] M. Roth,[2] S. H. Glenzer,[1] and M. Gauthier[1]

[1)] *SLAC National Accelerator Laboratory, Menlo Park, California 94025, USA*

[2)] *Institut für Kernphysik, Technische Universität Darmstadt, 64289 Darmstadt, Germany*

[3)] *Applied Physics Department, Stanford University, Stanford, California 94305, USA*

[4)] *Physics Department, Stanford University, Stanford, California 94305, USA*

[5)] *United States Military Academy, West Point, New York 10996, USA*

[6)] *Department of Electrical and Computer Engineering, University of Alberta, Edmonton, Alberta T6G 1H9, Canada*

(Dated: 2 August 2022)

High-power lasers can generate energetic particle beams and astrophysically-relevant pressure and temperature states in the high energy density (HED) regime. Recently commissioned high repetition rate (HRR) laser drivers are capable of producing these conditions at rates exceeding 1 Hz. However, experimental output from these systems is often limited by the difficulty of designing targets that match these repetition rates. To overcome this challenge, we have developed tungsten microfluidic nozzles which produce a continuously-replenishing jet that operates at flow speeds of approximately 10 m/s and can sustain shot frequencies up to 1 kHz. The ambient-temperature planar liquid jets produced by these nozzles can have thicknesses ranging from hundreds of nanometers to tens of microns. In this work we illustrate the operational principle of the microfluidic nozzle and describe its implementation in a vacuum environment. We provide evidence of successful laser-driven ion acceleration using this target and discuss the prospect of optimizing the ion acceleration performance through an in-situ jet thickness scan. Future applications for the jet throughout HED science include shock compression and studies of strongly-heated non-equilibrium plasmas. When fielded in concert with HRR-compatible laser, diagnostic, and active feedback technology, this target will facilitate advanced automated studies in HRR HED science, including machine learning-based optimization and high-dimensional statistical analysis.

I. INTRODUCTION

Until recently, reaching the pressures and tempera-tures of interest in high energy density (HED) science required high intensity lasers or pulsed-power drivers whose shot rates rapidly decreased with increasing en-ergy delivered to the target, limiting high-energy experi-ments to shot rates below 1 shot/hour. The emergence of laser drivers capable of operating at high repetition rate (HRR, $\geq$1 Hz) with drive energies of 10s of Joules will lead to dramatic changes to the study of HED science. It offers the capacity to increase experimental throughput a thousandfold or more and thus dramatically expands the rate at which new scientific knowledge can be obtained[1,2]. For sustained operation of target delivery systems at laser repetition rates, several conditions must be met[1,3]. Most importantly, the target must be refreshed quickly enough to provide an undisturbed surface for each laser pulse. The target delivery system must also be able to withstand repeated exposures to the extreme envi-ronments produced by the laser driver. Additionally, it should be compatible with vacuum system requirements and generate minimal debris. Finally, online optimizations of both laser and plasma properties are a promising method for efficiently navigating the highly coupled experimental parameter spaces characteristic of HED science. To perform these optimizations, it would be advantageous to use a target with the capacity to dynamically adjust key parameters such as thickness or density.

Various HRR-compatible target delivery systems have demonstrated a subset of these features. Solid target concepts include tape drives[4–7]based on Ti, Cu, Al, and CH foils and spinning disks[8,9], but these produce high levels of debris and are not dynamically adjustable. Cryogenic systems delivering jets[10–12] or droplets[13,14] have been used for HRR ion acceleration[15], but are limited to few to tens of µm thicknesses and require intricate platforms for efficient operation. Ambient-temperature systems delivering liquid droplets[16,17], free-standing films[18], or free-flowing jets[19–26] are simpler to operate and impose fewer constraints on the process fluid or resulting target geometry. Here we highlight two commonly used types of free-flowing jets: colliding jets[27–31], in which separate capillaries collide two individual jets to form a sheet jet, and converging jets[25,26], in which two flows within the same volume converge to form a sheet jet. Both approaches form a jet of a few millimeters in length with sub-µm to multiple µm thickness. While colliding jets can

[a)] These authors contributed equally to the work. Electronic mail: treffert@slac.stanford.edu, gdglenn@slac.stanford.edu

face alignment challenges due to the use of two independent capillaries, the single output aperture of converging jets facilitates alignment and operation.

In this work, we present a HRR-compatible, micron-scale, ambient-temperature, planar liquid jet target produced with tungsten microfluidic converging nozzles. This design builds on previous work[24–26] developing glass microfluidic converging nozzles for liquid-phase studies predominantly in biology or chemistry. Our nozzles are capable of sustained in-vacuum operation and produce jets composed of a series of liquid sheets with varying thickness across the length of each sheet. Tungsten nozzles are robust against the extreme environments generated in laser-target interactions with laser intensities exceeding 10^{21} W/cm^2 while achieving identical jet sizes and thicknesses to glass nozzles. In experiments using these jets, no target degradation or changes to the output surface of the nozzle were observed after thousands of shots. The flow velocity of the jet is approximately 10 m/s, supporting repetition rates up to the kHz level and separating irradiated regions by a distance of one cm or more. This target is therefore well-suited for advanced HRR experiments in a variety of fields ranging from shock compression to secondary source development. It will provide new opportunities to navigate the high-dimensional, highly-nonlinear parameter space of these experiments with statistical techniques and advances from machine learning. To illustrate the capabilities of the jet target, we show exemplary data from laser-driven proton and deuteron acceleration from water and heavy water jets to multi-MeV energies.

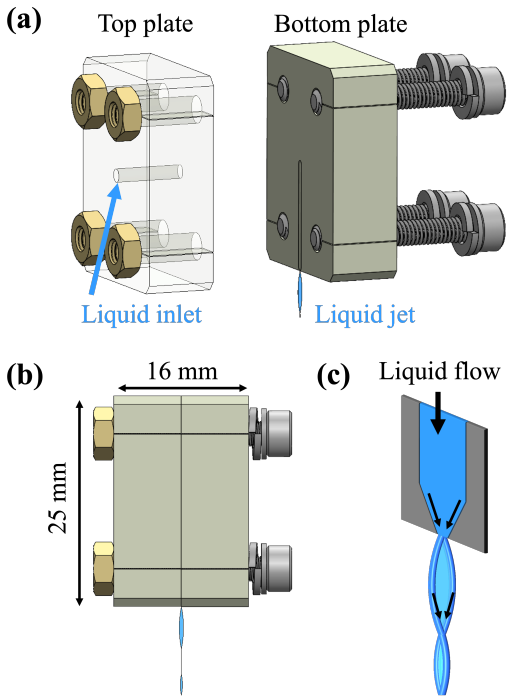

FIG. 1. (a) Exploded-view computer rendering of the hardware used to create the liquid jet. The microfluidic channel is etched into the bottom plate, and liquid enters through the inlet in the top plate. (b) Side view of the collapsed nozzle design and liquid jet. Note that the wide axis of the first sheet is perpendicular to the sealing plane between the top and bottom plate. (c) Schematic illustration of the nozzle geometry and the formation of the jet sheets as described in the text.

II. NOZZLE DESIGN

The HRR-compatible liquid jet is generated using a two-piece microfluidic nozzle assembly made of tungsten. As illustrated in Fig. 1, this design consists of a "top plate" and a "bottom plate." Initially, these components are identical "blank" plates. The sealing surface of each plate is polished to a peak-to-valley surface roughness of at most 300 nm using 1 µm diamond lapping disks. Precision micromachining is then used to bore the 1.6 mm diameter through hole used for the liquid inlet in the top plate and to etch a 25 µm deep converging microfluidic channel into the bottom plate.

To ensure a high-quality seal around the channel, the sealing surface of the bottom plate is coated with a 100 Å adhesive layer of titanium followed by a 500 nm thick layer of gold. Four through holes, one at each corner of the nozzle assembly, permit high-strength stainless steel fasteners to create a seal by exerting uniform pressure across the interface between the plates. Finally, the output surface of the nozzle assembly is polished to create a smooth transition between the plates and to ensure that the jet emerges perpendicular to the nozzle output surface. Liquid flow is maintained during the polishing process to ensure that removed material does not enter the channel and produce blockages.

As illustrated in Fig. 1(c), the internal channel geometry of the nozzle creates opposing, high-speed flows along the channel wall that converge at the nozzle exit. These flows then flatten the liquid from the center of the channel into a sheet perpendicular to the channel plane[25,26,31]. Surface tension ultimately overcomes the fluid inertia, preventing further lateral expansion of the sheet and collapsing its edges into rims with diameters of several tens of µm. With increasing distance from the nozzle the sheet narrows and grows thinner, resulting in a thickness gradient across the sheet. As the sheet continues to narrow, the rims ultimately recombine. Below the recombination point the jet expands into a subsequent, smaller sheet oriented orthogonally to the preceding sheet. Subsequent sheets are produced according to the same principle, growing successively smaller as energy dissipates through viscous effects in the "fluid chain" structure[29,32]. Eventually the rims no longer separate and the jet collapses into a cylinder after a maximum of 5 consecutive sheets with alternating perpendicular orientations.

III. JET OPERATION AND CHARACTERIZATION

During jet operation, constant liquid flow is applied throughout the nozzle assembly by a high pressure liquid chromatography (HPLC) pump (LC-20AD, Shimadzu Scientific Instruments). Depending on the flow rate setting, flow speeds of 10 m/s or higher allow operation of this target at repetition rates up to 1 kHz. The width and length of the sheets are proportional to the applied flow rate[26,33]. This relation holds until the flow rate reaches a critical value determined by the nozzle geometry, above which shear instabilities cause the primary sheet to fray into a spray of droplets and prevent the formation of the fluid chain. During operation, two large field of view imaging systems at approximately 110° to each other, as shown in Fig. 2, monitor the macroscopic structure of the jet continuously so these instabilities can be avoided.

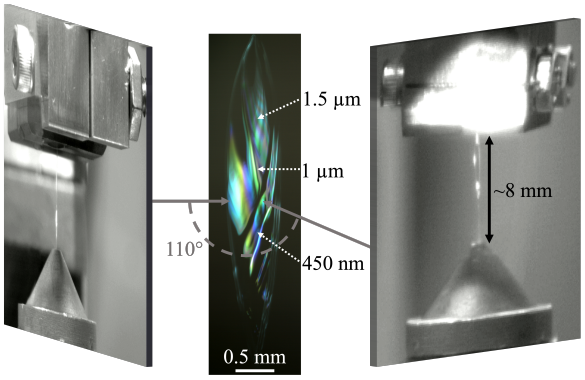

FIG. 2. Two large field of view cameras image the liquid jet at 110° from each other and enable precise alignment of the nozzle and catcher. The jet is collected by the catcher approx-imately 8 mm below the nozzle. A magnified view of the first sheet of the liquid jet is shown in the center using thin-film interferometry imaging. At a flow rate of 5–6 mL/min, the jet is up to 4 mm long, 0.7 mm wide and between 1.5 µm and 450 nm thick.

In-situ thin-film interferometry with either ultrafast, pulsed monochromatic illumination or time-integrated broadband illumination can provide precise measurements of the jet thickness as a function of distance from the nozzle. Unlike the overall jet dimensions, the thickness gradient across each sheet is determined by the nozzle geometry and is independent of the flow rate[26]. Here, the measurement was set up in reflection geometry at a 15° angle of incidence. The jet was illuminated with a broadband light source (Thorlabs LIUCWHA). Thin-film interferometry measures the interference of light reflected by both jet surfaces, the one facing towards and the one facing away from the light source. The resulting interference pattern is imaged using a 5x microscope objective (Thorlabs LMU-5X-NUV) and color CMOS camera (Allied Vision Mako G-223C). For constructive interference to occur between the two reflected waves, both surfaces (front and back) must be sufficiently flat in the area of interest. Depending on the jet thickness, different wavelengths in the white light source interfere constructively due to the differences in the optical path length. Consequently, the color of the detected light can be directly related to the thickness of the jet at a given point. While this technique is most effective for few-µm to sub-µm thicknesses, monochromatic light can be used to measure the thickness of thicker jets. Fig. 2 shows an image of the first sheet of a liquid jet produced using one of the tungsten nozzles with thicknesses ranging from 1.5 µm to 450 nm along the sheet. Ripples, usually appearing brighter and more white than other areas, are visible in the image and correspond to areas where the surface of the jet is slightly curved. Dark (black) regions are areas of high surface roughness. Previous work using glass nozzles has shown that surface nonuniformities similar to those depicted here can be associated with the roughness of the output surface and that smoother jets can be generated by modifying the output surface of the nozzles[26]. These techniques are under development for the tungsten nozzles to further improve the liquid sheet surface quality.

A. Operation Under Vacuum

During jet operation under vacuum rapid evaporation from the surface of the liquid target causes the jet to be surrounded by vapor. A heated in-vacuum catcher system collects the fluid and vapor 8 mm below the laser-target interaction point. This system allows the ultimate vacuum pressure to reach approximately 10^{-3} millibar under sustained jet operation (with only slight variations depending on flow rate). Liquid introduced into the vacuum chamber is efficiently evacuated and the amount of vapor generated is minimized by reducing the total surface area of liquid exposed to vacuum. This is necessary to ensure that the propagation of the drive laser will not be disturbed (e.g. by nonlinear effects such as Kerr lens-ing) and to protect sensitive components such as optical gratings or photoinjectors in connected vacuum volumes. The catcher assembly, made of C360 brass, consists of a hollow cylindrical body which narrows to a 500 µm orifice. The interior of the catcher body is connected to an external scroll pump via metal vacuum tubing to create a pressure difference between the two ends of the tubing. Heating the catcher body beyond 100° C to increase the temperature of the evacuated liquid and consequently the vapor pressure near the heated surface generates an additional pressure difference. The resulting pressure gradient assists gravity in evacuating the liquid vapor from the interior of the catcher, which is collected using both liquid and cold traps along the vacuum line outside the vacuum chamber.

High-intensity short-pulse laser systems require high vacuum in the laser compressor to protect the optical gratings. The vacuum pressures achieved during liquid jet operation are unsuitable for long-term operation of laser compressors due to increased risk of damage to the gratings on-shot. To mitigate this concern, we separate

the target and compressor chambers by placing a thin ($\leq$ 0.5 mm) fused silica vacuum isolation window between the two chambers[16]. The use of a thin optic minimizes B-integral and pulse broadening due to material dispersion, with values of $B < 0.5$ and pulse broadening of <5% achievable in practice. By using an antireflection-coated optic and placing the window at a slight angle, energy lost due to back reflections can be minimized and damage to the laser system from back-propagating pulses avoided.

IV. LASER-DRIVEN ION ACCELERATION

Early experiments studying the interaction of high-power, short-pulse lasers with thin planar targets demonstrated efficient ion acceleration through the robust, widely-studied target normal sheath acceleration (TNSA) mechanism[34–36], and subsequent studies explored alternative mechanisms both theoretically and experimentally[37–41]. Proof-of-principle work using liquid H_2O and D_2O jets produced by the tungsten microfluidic nozzles has demonstrated the generation of proton and deuteron beams with cutoff energies of several MeV. In these experiments, the third leaf of the jet was irradiated by the ALEPH laser at Colorado State University (400 nm, 5.5 J, 45 fs) focused onto the target using an f/2 off-axis parabola to a focal spot size of 1.8 µm full width half maximum (FWHM), yielding an intensity of 1.2×10^{21} W/cm^2. The target thickness was determined to be 5 ± 1 µm using measurements of jet thickness as a function of nozzle dimensions described in Ref. 26 and conservation of mass throughout the liquid jet. The energy spectra of the laser-accelerated ions were measured in the target normal direction using a Thomson parabola ion spectrometer equipped with a BAS-MS imaging plate (Fujifilm, Tokyo, Japan)[42,43] or a microchannel plate assembly (MCP) coupled with a phosphor screen imaged by a CCD camera.

Fig. 3(a) shows four deuteron energy spectra obtained from consecutive shot-on-demand laser-target interactions with a liquid D_2O jet[44]. The deuteron beams were detected using an MCP. All four traces show a cut-off energy between 1.8 and 1.9 MeV/nucleon and a semi-Maxwellian spectrum reaching a peak flux of 2×10^{11} deuterons/MeV/sr. The consistency of the cut-off energy and flux of these spectra demonstrates that the quality of the interaction was maintained throughout the shot series even after multiple high-intensity interactions. A larger dataset at the same laser conditions showed a standard error of 12% in the average deuteron flux at a sample energy of 1 MeV, further demonstrating the robustness of the target[44].

In Fig. 3(b), the fourth shot in the series shown in Fig. 3(a) is compared to the energy spectrum of protons accelerated from a liquid H_2O jet and measured using an image plate detector. The two spectra were obtained on different dates using different tungsten nozzles with the same channel dimensions and operated at similar flow rate settings. The laser interacted with the third leaf

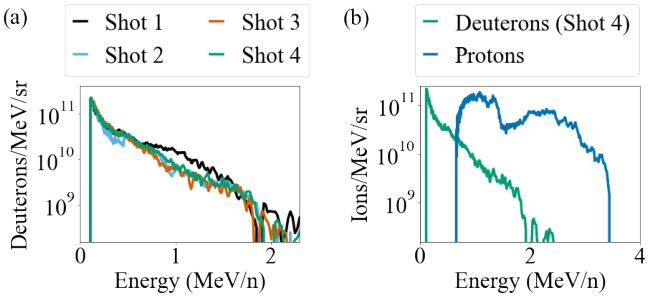

FIG. 3. (a) Consistent deuteron energy spectra across four consecutive laser shots demonstrate that the tungsten nozzle is not significantly degraded by repeated high-intensity laser-target interactions. Deuteron data presented in the figure above have been published with additional data demonstrating 0.5 Hz ion acceleration using the same target in Ref. 44. (b) Energy spectra of proton and deuteron beams accelerated by the interaction of a high-intensity laser with H_2O and D_2O sheet jets.

for both shots but at slightly different locations. Consequently, the D_2O jet was up to 1 µm thinner than the H_2O jet at the interaction point based on thin film interferometry measurements. Both the proton and the deuteron spectra exhibit a semi-Maxwellian distribution with peak fluxes above 10^{11} ions/MeV/sr. The proton spectrum shows a low energy cut-off energy of 0.65 MeV due to ion stopping in the protective layer of the image plate. The cutoff energy of the protons is approximately twice the cutoff energy of the deuterons.

This reduction in the ion cutoff energy for deuterons is consistent with the results of 2D particle-in-cell (PIC) OSIRIS[45,46] simulations of a high-intensity, high-temporal contrast laser interacting with liquid H_2O and D_2O jets. (Details of the simulation setup are provided in the Supplementary Material.) In Fig. 4, we show proton and deuteron energy spectra for different initial target thicknesses. The simulated laser pulse (400 nm, 10 J, 45 fs, 1.2 µm FWHM spot size) uses parameters achievable by frequency-doubling commercial petawatt-class lasers to improve the laser pulse contrast[47,48]. For the ultrathin liquid jet, high laser contrast is key to maintaining an undisturbed front surface before the arrival of the main laser pulse. Similar to the scaling observed experimentally, at a target thickness of 1 µm a factor of 2.25 higher cut-off energy is observed for protons compared to deuterons.

For both H_2O and D_2O jets, as the target thickness decreases the peak ion energy increases, reaches a maximum, and decreases. A variety of studies have theoretically and experimentally investigated the increases in proton cutoff energies observed with decreasing target thickness, finding that thin targets reduce the transverse spread of hot electrons inside the target and improve hot electron recirculation, thus increasing the rear-surface sheath field strength[49,50]. Additionally, when high-contrast laser systems and ultrathin (submicron)

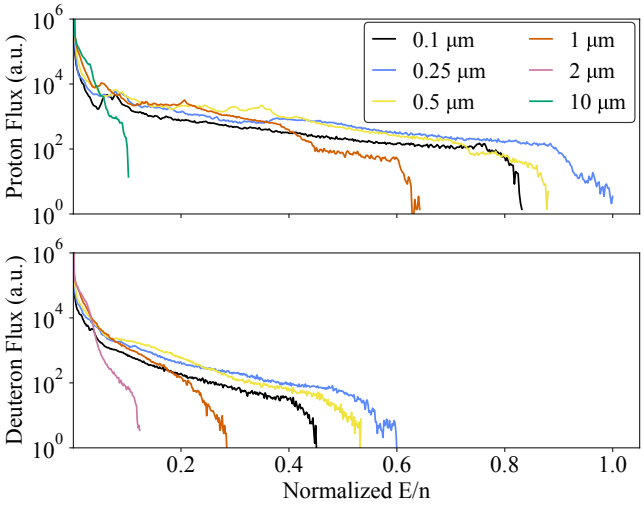

FIG. 4. Proton and deuteron energy spectra obtained from 2D PIC OSIRIS simulations of planar H_2O and D_2O jet targets irradiated by a high-power laser show the prospect of optimizing peak ion energies with online tuning of the jet thickness. Ion energies in MeV/nucleon have been normalized to the maximum energy obtained in the simulations.

targets are used, relativistic transparency effects can further enhance the ion acceleration process[37,38,41,51,52]. Our simulation results support the assumption of a transition between acceleration regimes for ultrathin jets by showing higher cut-off energies in those cases compared to μm thick jets. Thinner targets also exhibited reduced ion fluxes at low energies compared to thicker targets, further supporting the hypothesis that in these regimes, pre-accelerated low-energy ions were subsequently subjected to additional acceleration. Finally, the simulations show pronounced changes in the spatial emission profile for increasing target thicknesses, with lobes above and below the laser plane for thinner targets progressing to more uniform emission with increasing thickness. (For more information, see Figure S1 in the Supplementary Material.)

The liquid jet's capacity for tuning the thickness at the interaction point to submicron levels by simply translating the nozzle makes it a promising platform for studying the transition between different regimes of laser-driven ion acceleration. Fielding the liquid jet on currently-available laser systems therefore presents an opportunity to explore the large parameter space of target thickness and laser intensity illustrated in Fig. 5 and identify key acceleration mechanisms at play in various regions.

In future experiments, the liquid jet's capacity for HRR parameter scans will also make it possible to span the high-dimensional space of laser and target parameters with unprecedented precision, providing validation of experimentally-observed scaling relations[36,53]. Online diagnostic feedback and automated control of experimental parameters using tools such as genetic algorithms[54] or Bayesian optimization[55,56] will accelerate decision-making and consequently the efficiency of searches for experimental optima. The optimizer can be tuned to achieve improvements in parameters of interest for applications, such as peak ion energy and flux, beam divergence, and spectral bandwidth. The optimal experimental parameters can then be modeled computationally in order to clarify the microphysics underlying the observed acceleration performance[55].

V. ADDITIONAL APPLICATIONS

As HED science increasingly leverages HRR-capable x-ray free electron lasers (XFELs), shock drivers, and high-power lasers, target systems compatible with HRR operation will become essential. The robustness of the liquid jet to the extreme environments of high-power laser-matter interactions makes it suitable for use with a wide range of laser pulse energies and durations. Consequently, this target can be used in a variety of HRR studies relevant to HED science. In these studies, the HRR target will be key to enabling the collection of dramatically larger datasets or finer parameter scans. Additionally, these studies can take advantage of the liquid jet's capacity to deliver thicknesses from hundreds of nm to tens of μm and ability to operate with various process fluids. We feature applications throughout HED science, including shock compression, ultrafast heating, and radiation generation physics.

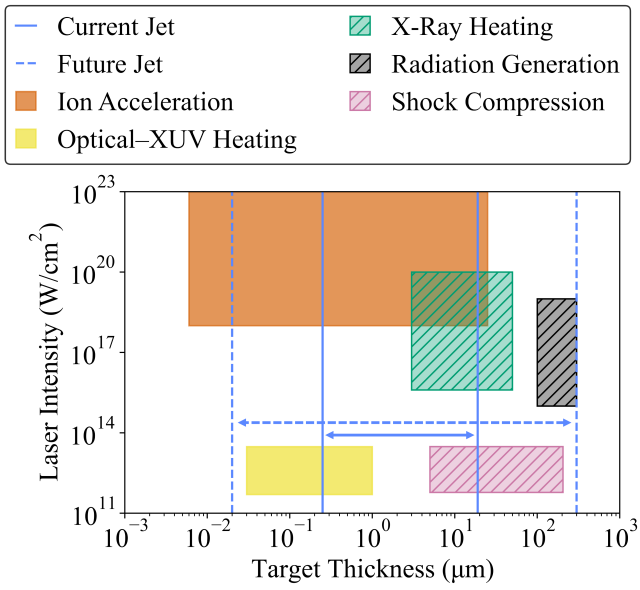

FIG. 5. Plot of laser intensity vs. target thickness showing achievable liquid jet thicknesses and the approximate target thicknesses and laser intensities typically of interest for studies in several areas of HED science and related fields. Current capabilities are shown in solid color and future capabilities are indicated with dashed lines or crosshatching.

A. Shock Compression

When the liquid jet target is operated with thicknesses of tens of µm or more (achievable with the current design), it is well-suited for HRR shock compression studies at pressures of tens of GPa and higher. These conditions are relevant to planetary interiors[57,58]. Liquid mixtures can be used to reproduce the atomic ratios of icy giant planetary interiors in order to study their internal structures and unusual magnetic fields[59,60]. The planar geometry of the jet helps produce a well-defined shock state and allows the shock conditions to be monitored by VISAR diagnostics, facilitating comparison to theoretical modeling. Until recently, the high-energy, nanosecond-duration lasers required to shock-compress materials to GPa pressures generally operated at repetition rates of one shot/several minutes, even with liquid targets[60,61]. However, HRR shock drivers matching the jet's repetition rate capabilities are becoming available at a variety of facilities, including the HiLASE Center[62], the European X-Ray Free-Electron Laser[63], and the upcoming MEC-U facility at the Linac Coherent Light Source (LCLS)[64].

B. Ultrafast Heating

Ultrafast (fs-scale) heating of the liquid jet with intense extreme ultraviolet (XUV) or x-ray pulses can be used to study highly nonequilibrium states of liquids. While the nonequilibrium ultrafast dynamics of strongly-excited solids are increasingly being studied with x-ray free electron lasers (XFELs)[65–67], measurements of strongly-excited liquids on fs–ps timescales remain rare[68,69]. These studies provide insight into the fundamental properties of liquid compounds in extreme pressure and temperature environments and clarify their influence on scattering signals when used as sample environments in XFEL studies. In both cases, the optimal sample thickness is determined by the skin depth of the heating radiation. As shown in Fig. 5, radiation up to XUV energies can efficiently excite liquid jets with thicknesses up to several hundred nm[69]. Highly penetrating hard x-rays can heat jets with thicknesses up to tens of µm, generating larger volumes of heated material and allowing a wider region of k-space to be accessed with diffraction on a single shot.

C. Radiation Generation

Another application of the liquid jet is the production of secondary radiation ranging from THz to x-rays. THz radiation is commonly generated via optical rectification of ultrafast laser pulses in solid nonlinear media, but recent work has shown that laser-driven ionization of planar liquid water jets can be a high-efficiency source of THz radiation[70–72]. In continuously-refreshing jets, material damage from high pump laser intensities ceases to be a concern. Additionally, reduced absorption from phonons makes laser irradiation of liquid jets a promising approach for high-energy, broadband THz pulse generation. Ionization in a liquid jet is also key to the x-ray laser oscillator (XLO) concept. Photoionization in a liq-uid gain medium by a seed pulse from an XFEL pro-duces amplified spontaneous emission in an x-ray cavity. $K\alpha_1$ signal radiation circulates in the cavity and interacts with subsequent XFEL pulses in the jet, ultimately pro-ducing coherent x-ray lasing with time-bandwidth prod-ucts down to 1.8 eV fs and $> 5 \times 10^{10}$ photons/pulse[73]. In both of these cases, planar jets with thicknesses of 100–300 µm balance radiation generation with absorp-tion in the gain medium, and the use of varied process fluids is of interest for tuning the output pulse energy or frequency[71,73]. Additional development and adapta-tion of the nozzle design described here will make this thickness range accessible to jets produced by converging tungsten nozzles, providing an alternative to the dye laser jets or non-converging cylindrical jets previously consid-ered for these applications[73,74].

VI. CONCLUSION AND OUTLOOK

We have demonstrated an ambient-temperature liquid jet target with several key properties that make it well-suited for HRR studies in HED science. The jet consists of planar sheets with alternating orientation and thicknesses that decrease with increasing distance from the nozzle. Different nozzle geometries provide access to thicknesses ranging from hundreds of nm to tens of µm. The jet is compatible with in-vacuum operation and can be operated with a variety of process fluids. Combined with its inherently HRR nature, this target is a compelling option for experiments including, but not limited to, machine learning optimization of laser-driven ion acceleration and shock-compression studies reaching planetary interior conditions.

The tungsten microfluidic nozzles, which have been shown to be robust against laser intensities above 10^{21} W/cm^2, and the catcher assembly used to create and efficiently evacuate the liquid jet are key to the platform. By collecting the jet with a heated in-vacuum catcher system, we significantly reduce residual vapor levels during jet operation and thus mitigate spatiotemporal distortions to the drive laser. The use of a thin vacuum isolation window can further separate vapor from delicate optical components such as the compressor gratings of a high-power short-pulse laser system.

An initial experiment implementing µm-thick liquid H_2O and D_2O targets at the ALEPH laser at Colorado State University showed proton and deuteron acceleration to MeV-scale energies. Repeated irradiation of the liquid D_2O jet accelerated deuterons in four consecutive shots with minimal differences in cut-off energy and generated deuteron flux. Simulations performed using the

2D PIC code OSIRIS suggest a transition to an alternative acceleration regime for sub-µm thick liquid targets.

Ongoing development efforts and adaptation of existing nozzle designs will allow us to extend the thickness range accessible with the jet from tens of nm to hundreds of µm. This advance will enable the jet to be used as a HRR source of energetic THz and high-brightness x-ray pulses. It will also facilitate studies of liquid-phase ionization dynamics with higher pump laser fluences than have previously been achievable[75,76] and investigations of supercooled water using transient x-ray absorption spectroscopy or ultrafast electron diffraction[77]. Additional plans for this target delivery system include the development of multilayered jets (preliminarily described in Ref. 78) for ultrafast mixing experiments and jets doped with nanoparticles for studies of catalysis[79] or nanofabrication[80]. Supplementing this unique target with HRR-compatible laser, diagnostic, and feedback technologies will yield significant improvements in experimental data quantity and quality and thereby advance the state of the art in multiple domains of HED science.

SUPPLEMENTARY MATERIAL

The supplementary material provides details of the setup of our PIC simulations and additional discussion of the simulation results.

ACKNOWLEDGEMENTS

The authors thank C. A. J. Palmer, M. J. V. Streeter, N. Bourgeois, E. E. McBride and M. Z. Mo for helpful conversations. We additionally thank J. J. Rocca and his group at Colorado State University for their experimental support. This work was supported by the U.S. Department of Energy (DOE) Office of Science, Fusion Energy Sciences under FWP 100182 and LaserNetUS DE-SC0021246. This research used the resources of SLAC National Accelerator Laboratory, supported by the U.S. Department of Energy, Office of Science, Office of Basic Energy Sciences under Contract No. DE-AC02-76SF00515. This work was also partially supported by the National Science Foundation under Grant No. 1903414. The authors acknowledge the OSIRIS Consortium, consisting of UCLA and IST (Portugal) for the use of the OSIRIS 4.0 framework. Simulations were run on Cori (NERSC) through an ALCC award. F. T. acknowledges partial support from the National Nuclear Security Administration (NNSA). G. D. G. acknowledges support from the U.S. DOE NNSA SSGF program under DE-NA0003960. The work of C. B. C. was partially supported by the Natural Sciences and Engineering Research Council of Canada (NSERC).

AUTHOR DECLARATIONS

Conflict of Interest

The authors have no conflicts to disclose.

DATA AVAILABILITY

The data that support the findings of this study are available from the corresponding author upon reasonable request.

REFERENCES

[1]T. Ma, D. Mariscal, R. Anirudh, T. Bremer, B. Z. Djordjevic, T. Galvin, E. Grace, S. Herriot, S. Jacobs, B. Kailkhura, et al., Plasma Physics and Controlled Fusion **63** (2021), 10.1088/1361-6587/ac1f67.

[2]P. W. Hatfield, J. A. Gaffney, G. J. Anderson, S. Ali, L. Antonelli, S. Başeğmez du Pree, J. Citrin, M. Fajardo, P. Knapp, B. Kettle, et al., Nature **593**, 351 (2021).

[3]I. Prencipe, J. Fuchs, S. Pascarelli, D. W. Schumacher, R. B. Stephens, N. B. Alexander, R. Briggs, M. Büscher, M. O. Cernaianu, A. Choukourov, et al., High Power Laser Science and Engineering **5** (2017), 10.1017/hpl.2017.18.

[4]P. McKenna, K. W. Ledingham, I. Spencer, T. McCany, R. P. Singhal, C. Ziener, P. S. Foster, E. J. Divall, C. J. Hooker, D. Neely, et al., Review of Scientific Instruments **73**, 4176 (2002).

[5]T. Nayuki, Y. Oishi, T. Fujii, K. Nemoto, T. Kayoiji, Y. Okano, Y. Hironaka, K. G. Nakamura, K. I. Kondo, and K. I. Ueda, Review of Scientific Instruments **74**, 3293 (2003).

[6]S. Steinke, J. H. Bin, J. Park, Q. Ji, K. Nakamura, A. J. Gonsalves, S. S. Bulanov, M. Thévenet, C. Toth, J. L. Vay, et al., Physical Review Accelerators and Beams **23**, 1 (2020).

[7]F. P. Condamine, N. Jourdain, J.-C. Hernandez, M. Taylor, H. Bohlin, A. Fajstavr, T. M. Jeong, D. Kumar, T. Laštovička, O. Renner, et al., Review of Scientific Instruments **92**, 063504 (2021).

[8]B. Hou, J. Nees, J. Easter, J. Davis, G. Petrov, A. Thomas, and K. Krushelnick, Applied Physics Letters **95**, 3 (2009).

[9]Y. Gershuni, D. Roitman, I. Cohen, E. Porat, Y. Danan, M. Elkind, A. Levanon, R. Louzon, D. Reichenberg, A. Tsabary, et al., Nuclear Instruments and Methods in Physics Research, Section A: Accelerators, Spectrometers, Detectors and Associated Equipment **934**, 58 (2019).

[10]J. B. Kim, S. Göde, and S. H. Glenzer, Review of Scientific Instruments **87** (2016), 10.1063/1.4961089.

[11]C. B. Curry, C. Schoenwaelder, S. Goede, J. B. Kim, M. Rehwald, F. Treffert, K. Zeil, S. H. Glenzer, and M. Gauthier, Journal of Visualized Experiments **2020**, 1 (2020).

[12]D. Margarone, A. Velyhan, J. Dostal, J. Ullschmied, J. P. Perin, D. Chatain, S. Garcia, P. Bonnay, T. Pisarczyk, R. Dudzak, et al., Physical Review X **6** (2016), 10.1103/PhysRevX.6.041030.

[13]B. Aurand, K. M. Schwind, T. Toncian, E. Aktan, M. Cerchez, L. Lessmann, C. Mannweiler, R. Prasad, A. Khoukaz, and O. Willi, New Journal of Physics **22** (2020), 10.1088/1367-2630/ab7bf0.

[14]T. Ditmire, J. Zweiback, V. P. Yanovsky, T. E. Cowan, G. Hays, and K. B. Wharton, Nature **398**, 489 (1999).

[15]M. Gauthier, C. B. Curry, S. Göde, F.-E. Brack, J. B. Kim, M. J. MacDonald, J. Metzkes, L. Obst, M. Rehwald, C. Rödel, et al., Applied Physics Letters **111** (2017), 10.1063/1.4990487.

[16]B. Aurand, E. Aktan, K. M. Schwind, R. Prasad, M. Cerchez, T. Toncian, and O. Willi, Laser and Particle Beams , 1 (2020).

[17]M. Schnürer, S. Ter-Avetisyan, S. Busch, E. Risse, M. P. Kalachnikov, W. Sandner, and P. V. Nickles, Laser and Particle Beams **23**, 337 (2005).

[18]P. L. Poole, C. Willis, G. E. Cochran, R. T. Hanna, C. D. Andereck, and D. W. Schumacher, Applied Physics Letters **109** (2016), 10.1063/1.4964841.

[19]J. Hah, G. M. Petrov, J. A. Nees, Z. H. He, M. D. Hammig, K. Krushelnick, and A. G. Thomas, Applied Physics Letters **109**, 144102 (2016).

[20]J. T. Morrison, S. Feister, K. D. Frische, D. R. Austin, G. K. Ngirmang, N. R. Murphy, C. Orban, E. A. Chowdhury, and W. M. Roquemore, New Journal of Physics **20**, 069501 (2018).

[21]K. M. George, J. T. Morrison, S. Feister, G. K. Ngirmang, J. R. Smith, A. J. Klim, J. Snyder, D. Austin, W. Erbsen, K. D. Frische, et al., High Power Laser Science and Engineering **7**, e50 (2019).

[22]A. Zymakova, M. Albrecht, R. Antipenkov, A. Spacek, S. Karatodorov, O. Hort, J. Andreasson, and J. Uhlig, Journal of Synchrotron Radiation **28**, 1778 (2021).

[23]P. Puyuelo-Valdes, D. de Luis, J. Hernandez, J. I. Apiñaniz, A. Curcio, J. L. Henares, M. Huault, J. A. Pérez-Hernández, L. Roso, G. Gatti, et al., Plasma Physics and Controlled Fusion **64**, 054003 (2022).

[24]J. D. Koralek, J. B. Kim, P. Brůža, C. B. Curry, Z. Chen, H. A. Bechtel, A. A. Cordones, P. Sperling, S. Toleikis, J. F. Kern, et al., Nature Communications **9** (2018), 10.1038/s41467-018-03696-w.

[25]B. Ha, D. P. Deponte, and J. G. Santiago, Physical Review Fluids **3**, 1 (2018).

[26]C. J. Crissman, M. Mo, Z. Chen, J. Yang, D. A. Huyke, S. H. Glenzer, K. Ledbetter, J. P. F. Nunes, M. L. Ng, H. Wang, et al., Lab on a Chip **22**, 1365 (2022).

[27]D. Hasson and R. E. Peck, AIChE Journal **10**, 752 (1964), https://aiche.onlinelibrary.wiley.com/doi/pdf/10.1002/aic.690100533.

[28]Y. J. Choo and B. S. Kang, Experiments in Fluids **31**, 56 (2001).

[29]J. W. Bush and A. E. Hasha, Journal of Fluid Mechanics **511**, 285 (2004).

[30]M. Ekimova, W. Quevedo, M. Faubel, P. Wernet, and E. T. J. Nibbering, Structural Dynamics **2**, 054301 (2015), https://doi.org/10.1063/1.4928715.

[31]V. Sanjay and A. K. Das, Physics of Fluids **29** (2017), 10.1063/1.4998288.

[32]S. Jung, S. D. Hoath, G. D. Martin, and I. M. Hutchings, Physics of Fluids **22**, 1 (2010).

[33]E. Villermaux and C. Clanet, Journal of Fluid Mechanics **462**, 341 (2002).

[34]R. A. Snavely, M. H. Key, S. P. Hatchett, I. E. Cowan, M. Roth, T. W. Phillips, M. A. Stoyer, E. A. Henry, T. C. Sangster, M. S. Singh, et al., Physical Review Letters **85**, 2945 (2000).

[35]A. Maksimchuk, S. Gu, K. Flippo, D. Umstadter, and A. Y. Bychenkov, Physical Review Letters **84**, 4108 (2000).

[36]S. C. Wilks, A. B. Langdon, T. E. Cowan, M. Roth, M. Singh, S. Hatchett, M. H. Key, D. Pennington, A. MacKinnon, and R. A. Snavely, Physics of Plasmas **8**, 542 (2001).

[37]A. P. Robinson, M. Zepf, S. Kar, R. G. Evans, and C. Bellei, New Journal of Physics **10** (2008), 10.1088/1367-2630/10/1/013021, arXiv:0708.2040.

[38]L. Yin, B. J. Albright, B. M. Hegelich, and J. C. Fernandez, Laser and Particle Beams **24**, 291 (2006).

[39]D. Haberberger, S. Tochitsky, F. Fiuza, C. Gong, R. A. Fonseca, L. O. Silva, W. B. Mori, and C. Joshi, Nature Physics **8**, 95 (2012).

[40]F. Fiuza, A. Stockem, E. Boella, R. A. Fonseca, L. O. Silva, D. Haberberger, S. Tochitsky, C. Gong, W. B. Mori, and C. Joshi, Physical Review Letters **109**, 1 (2012), arXiv:1206.2903.

[41]R. Mishra, F. Fiuza, and S. Glenzer, New Journal of Physics **20** (2018), 10.1088/1367-2630/aab8db.

[42]A. Mancic et al., Rev. Sci. Instrum. **79**, 073301 (2008).

[43]I. W. Choi et al., Meas. Sci. Technol. **20**, 115112 (2009).

[44]F. Treffert, C. B. Curry, H.-G. J. Chou, C. Crissman, D. P. Deponte, F. Fiuza, G. D. Glenn, R. Hollinger, R. Nedbailo, J. Park, et al., Applied Physics Letters (In Press).

[45]R. A. Fonseca, L. O. Silva, F. S. Tsung, V. K. Decyk, W. Lu, C. Ren, W. B. Mori, S. Deng, S. Lee, T. Katsouleas, et al., Lecture Notes in Computer Science (including subseries Lecture Notes in Artificial Intelligence and Lecture Notes in Bioinformatics) **2331 LNCS**, 342 (2002).

[46]R. A. Fonseca, S. F. Martins, L. O. Silva, J. W. Tonge, F. S. Tsung, and W. B. Mori, Plasma Physics and Controlled Fusion **50** (2008), 10.1088/0741-3335/50/12/124034, arXiv:0810.2460.

[47]K. Nakamura, H. S. Mao, A. J. Gonsalves, H. Vincenti, D. E. Mittelberger, J. Daniels, A. Magana, C. Toth, and W. P. Leemans, IEEE Journal of Quantum Electronics **53** (2017), 10.1109/JQE.2017.2708601.

[48]Y. Wang, S. Wang, A. Rockwood, B. M. Luther, R. Hollinger, A. Curtis, C. Calvi, C. S. Menoni, and J. J. Rocca, Opt. Lett. **42**, 3828 (2017).

[49]A. J. Mackinnon, Y. Sentoku, P. K. Patel, D. W. Price, S. Hatchett, M. H. Key, C. Andersen, R. Snavely, and R. R. Freeman, Phys. Rev. Lett. **88**, 215006 (2002).

[50]D. Neely, P. Foster, A. Robinson, F. Lindau, O. Lundh, A. Persson, C.-G. Wahlström, and P. McKenna, Applied Physics Letters **89**, 021502 (2006), https://doi.org/10.1063/1.2220011.

[51]P. L. Poole, L. Obst, G. E. Cochran, J. Metzkes, H. P. Schlenvoigt, I. Prencipe, T. Kluge, T. Cowan, U. Schramm, D. W. Schumacher, et al., New Journal of Physics **20** (2018), 10.1088/1367-2630/aa9d47.

[52]A. Higginson, R. J. Gray, M. King, R. J. Dance, S. D. Williamson, N. M. Butler, R. Wilson, R. Capdessus, C. Armstrong, J. S. Green, et al., Nature Communications **9** (2018), 10.1038/s41467-018-03063-9.

[53]M. Zimmer, S. Scheuren, T. Ebert, G. Schaumann, B. Schmitz, J. Hornung, V. Bagnoud, C. Rödel, and M. Roth, Physical Review E **104**, 045210 (2021).

[54]S. J. D. Dann, C. D. Baird, N. Bourgeois, O. Chekhlov, S. Eardley, C. D. Gregory, J.-N. Gruse, J. Hah, D. Hazra, S. J. Hawkes, et al., Physical Review Accelerators and Beams **22**, 041303 (2019).

[55]R. J. Shalloo, S. J. Dann, J. N. Gruse, C. I. Underwood, A. F. Antoine, C. Arran, M. Backhouse, C. D. Baird, M. D. Balcazar, N. Bourgeois, et al., Nature Communications **11**, 0 (2020), arXiv:2007.14340.

[56]S. Jalas, M. Kirchen, P. Messner, P. Winkler, L. Hübner, J. Dirkwinkel, M. Schnepp, R. Lehe, and A. R. Maier, Physical Review Letters **126**, 104801 (2021).

[57]D. Kraus, J. Vorberger, A. Pak, N. J. Hartley, L. B. Fletcher, S. Frydrych, E. Galtier, E. J. Gamboa, D. O. Gericke, S. H. Glenzer, et al., Nature Astronomy **1**, 606 (2017).

[58]N. J. Hartley, S. Brown, T. E. Cowan, E. Cunningham, T. Döppner, R. W. Falcone, L. B. Fletcher, S. Frydrych, E. Galtier, E. J. Gamboa, et al., Scientific Reports **9**, 1 (2019).

[59]W. J. Nellis, N. C. Holmes, A. C. Mitchell, D. C. Hamilton, and M. Nicol, Journal of Chemical Physics **107**, 9096 (1997).

[60]M. Guarguaglini, J. A. Hernandez, T. Okuchi, P. Barroso, A. Benuzzi-Mounaix, M. Bethkenhagen, R. Bolis, E. Brambrink, M. French, Y. Fujimoto, et al., Scientific Reports **9**, 1 (2019).

[61]A. E. Gleason, C. A. Bolme, E. Galtier, H. J. Lee, E. Granados, D. H. Dolan, C. T. Seagle, T. Ao, S. Ali, A. Lazicki, et al., Physical Review Letters **119**, 1 (2017).

[62]P. Mason, M. Divoký, K. Ertel, J. Pilař, T. Butcher, M. Hanuš, S. Banerjee, J. Phillips, J. Smith, M. De Vido, et al., Optica **4**, 438 (2017).

[63]U. Zastrau, K. Appel, C. Baehtz, O. Baehr, L. Batchelor, A. Berghäuser, M. Banjafar, E. Brambrink, V. Cerantola, T. E. Cowan, et al., Journal of Synchrotron Radiation **28**, 1393 (2021).

[64]G. Dyer, "Matter in Extreme Conditions Upgrade Conceptual Design Report," Tech. Rep. (SLAC National Accelerator Laboratory (SLAC), Menlo Park, CA (United States), 2022).

[65]A. Lévy, P. Audebert, R. Shepherd, J. Dunn, M. Cammarata, O. Ciricosta, F. Deneuville, F. Dorchies, M. Fajardo, C. Fourment, et al., Physics of Plasmas **22**, 030703 (2015).
[66]I. Inoue, Y. Inubushi, T. Sato, K. Tono, T. Katayama, T. Kameshima, K. Ogawa, T. Togashi, S. Owada, Y. Amemiya, et al., Proceedings of the National Academy of Sciences of the United States of America **113**, 1492 (2016).
[67]N. J. Hartley, J. Grenzer, L. Huang, Y. Inubushi, N. Kamimura, K. Katagiri, R. Kodama, A. Kon, W. Lu, M. Makita, et al., Physical Review Letters **126**, 1 (2021), arXiv:2007.15007.
[68]K. R. Beyerlein, H. O. Jönsson, R. Alonso-Mori, A. Aquila, S. Bajt, A. Barty, R. Bean, J. E. Koglin, M. Messerschmidt, D. Ragazzon, et al., Proceedings of the National Academy of Sciences of the United States of America **115**, 5652 (2018).
[69]Z. Chen, X. Na, C. B. Curry, S. Liang, M. French, A. Descamps, D. P. Deponte, J. D. Koralek, J. B. Kim, S. Lebovitz, et al., Matter and Radiation at Extremes **6** (2021), 10.1063/5.0043726.
[70]Q. Jin, Y. E, K. Williams, J. Dai, and X. C. Zhang, Applied Physics Letters **111** (2017), 10.1063/1.4990824.
[71]A. N. Tcypkin, E. A. Ponomareva, S. E. Putilin, S. V. Smirnov, S. A. Shtumpf, M. V. Melnik, Y. E, S. A. Kozlov, and X.-C. Zhang, Optics Express **27**, 15485 (2019), arXiv:1903.12425.
[72]Y. E, Q. Jin, A. Tcypkin, and X. C. Zhang, Applied Physics Letters **113** (2018), 10.1063/1.5054599.
[73]A. Halavanau, A. Benediktovitch, A. A. Lutman, D. DePonte, D. Cocco, N. Rohringer, U. Bergmann, and C. Pellegrini, Proceedings of the National Academy of Sciences of the United States of America , 1 (2020).
[74]E. A. Ponomareva, A. O. Ismagilov, S. E. Putilin, A. N. Tsypkin, S. A. Kozlov, and X.-C. Zhang, Communications Physics **4**, 4 (2021).
[75]M. F. Lin, N. Singh, S. Liang, M. Mo, J. P. Nunes, K. Ledbetter, J. Yang, M. Kozina, S. Weathersby, X. Shen, et al., Science **374**, 92 (2021).
[76]J. P. Nunes, K. Ledbetter, M. Lin, M. Kozina, D. P. Deponte, E. Biasin, M. Centurion, C. J. Crissman, M. Dunning, S. Guillet, et al., Structural Dynamics **7** (2020), 10.1063/1.5144518.
[77]Y. P. Chang, Z. Yin, T. Balciunas, H. J. Wörner, and J. P. Wolf, Structural Dynamics **9** (2022), 10.1063/4.0000139, arXiv:2112.05466.
[78]D. J. Hoffman, H. A. Bechtel, D. A. Huyke, J. G. Santiago, D. P. Deponte, and J. D. Koralek, arXiv (2022), arXiv:2203.08784.
[79]E. Cortés, W. Xie, J. Cambiasso, A. S. Jermyn, R. Sundararaman, P. Narang, S. Schlücker, and S. A. Maier, Nature Communications **8**, 1 (2017).
[80]S. Hashimoto, D. Werner, and T. Uwada, Journal of Photochemistry and Photobiology C: Photochemistry Reviews **13**, 28 (2012).